

National Transonic Facility Public Geometry Release and Summary

Brent W. Pomeroy,* Melissa B. Rivers,[†] Eric L. Walker[‡]
NASA Langley Research Center, Hampton, VA, 23681

Scott E. Brynildsen,[§] Norma L. Farr[¶]
Analytical Mechanics Associates, Hampton, VA, 23681

Ben J. Rider^{||}
Boeing Commercial Airplanes, Everett, WA, 98204

Seyedeh Sheida Hosseini**
NASA Ames Research Center, Moffett Field, CA, 94035

This paper highlights the recent release of the NASA National Transonic Facility high-speed leg geometry and gives an overview of the experimental facility with a brief discussion of the released geometry. A detailed laser scan of the facility yielded a point cloud of data points from which high-quality computer aided design surfaces were generated. The resulting loft, currently denoted as NTF_highspeedleg_definition_v1p9 released in June 2025, includes the inlet, contraction, test section, wall slots, upper swept strut, arc sector, and diffuser. The geometry, which is posted on the Drag Prediction Workshop website (currently at <https://aiaa-dpw.larc.nasa.gov/ntf.html>), has been approved for public use. It is hoped that high-quality simulations of an experimental model in the test section will help quantify the effect of the test environment relative to free-air computational simulations.

I. Nomenclature

cm	=	centimeter
C	=	degrees Celsius
F	=	degrees Fahrenheit
ft	=	foot
in	=	inch
K	=	kelvin
m	=	meter
psi	=	pound force per square inch
O	=	origin for axis of rotation
R	=	a rotation matrix
t _s	=	standoff thickness (in)
v	=	a vector
α	=	angle of attack (deg)
θ	=	an angle (deg)

Acronyms

*Aerodynamics Research Engineer, Configuration Aerodynamics Branch, AIAA Senior Member.

[†]Reduced Life Cycle Cost Subproject Manager, Transformational Tools and Technologies Project, AIAA Associate Fellow.

[‡]Chief Engineer for Test Operation Excellence, Research Directorate Chief Engineer Council Chair, AIAA Associate Fellow.

[§]Geometry Laboratory Group Engineer, Research, Science, & Engineering Services.

[¶]Geometry Laboratory Group Lead, Research, Science, & Engineering Services, AIAA Member.

^{||}High-Speed Aerodynamics Engineer, High-Speed Aerodynamics, Flight Sciences, AIAA Senior Member.

^{**}Reduced Life Cycle Cost Subproject Deputy Manager, Transformational Tools and Technologies Project, AIAA Member.

AC	= Analysis Coordinate System
AGARD	= Advisory Group for Aerospace Research and Development
AIAA	= American Institute of Aeronautics and Astronautics
CAD	= Computer-Aided Design
CRM	= Common Research Model
CRM-HL	= High Lift Common Research Model
CRM-NLF	= Natural Laminar Flow Common Research Model
DPW	= Drag Prediction Workshop
FS	= Full Scale Vehicle Coordinate System
LaRC	= Langley Research Center
NASA	= National Aeronautics and Space Administration
NTF	= National Transonic Facility
ONERA	= Office National d'Études et de Recherches Aérospatiales
MS	= Model Scale Vehicle Coordinate System
WT	= Wind Tunnel Coordinate System
ZA	= Wind Tunnel Coordinate System with Vehicle at $\alpha=0$ deg
14x22	= NASA LaRC 14- by 22-Foot Subsonic Tunnel

II. Facility Overview and History

The National Transonic Facility (NTF) at National Aeronautics and Space Administration (NASA) Langley Research Center (LaRC) in Hampton, Virginia is a unique facility with specialized testing capability. Since the 1980s, the NTF has been used for a large number of launch and air vehicle experiments. The fan-driven, closed-circuit facility is the world's largest pressurized, cryogenic wind tunnel, and one of only a few facilities in the world that can simultaneously match transonic Mach number and aircraft flight Reynolds number. The NTF permits the largest range of Reynolds numbers in the world, making the facility globally unique. The facility can be run at either cryogenic temperatures with nitrogen or ambient temperatures with dry air. A detailed overview of the tunnel characteristics is shown in Table 1 [1]. Both full-span and semispan models can be tested in the wind tunnel, and a wide variety of instrumentation, including optical equipment, can be used in the facility. Great care has been taken to achieve high-quality flow in the test section. In particular, the 14.95-to-1 contraction ratio and four different damping screens decrease the freestream turbulence in the test section and improve overall flow quality. Disturbances from the drive fan are minimized through acoustic treatment upstream and downstream of the fan.

Table 1 Key Facility Characteristics

Test Section Dimensions	8.2 ft high by 8.2 ft wide by 25 ft long
Area	66.8 ft ²
Speed	Mach 0.1 to 1.2
Reynolds Number	4 to 145×10^6 per foot
Temperature	-250 to 130 deg Fahrenheit
Pressure	15 to 130 psi
Test Gas	Dry air and also nitrogen
Circuit Length	497 ft
Drive Power	135,000 horsepower
Contraction area ratio	14.95:1

The facility, which was declared fully operational in 1984, was designed, constructed, and tested in five phases: 1) establish the need for a high Reynolds number test facility, 2) perform conceptual design yielding the cryogenic nitrogen concept, 3) finalize detailed design, 4) construct facility and plan research project tests, and 5) develop operation methods and research applications [2–5]. High Reynolds number testing was desired for risk reduction such that vehicle

performance and characteristics could be more accurately predicted in the design environment. These risk-reduction efforts would avoid expensive and laborious late-product-cycle design changes, which was observed for at least five flight vehicle programs [6].

While high Reynolds number aerodynamic data were desired for decades before the NTF was constructed, the formal need was not determined to be a national priority until the mid-to-late 1960s [7]. At the time, an international need for flight Reynolds number testing had been established. A facility-needs exercise commenced in the mid 1960s to identify facility characteristics that would facilitate transonic, high Reynolds number conditions. These facility requirements were matured by the US Department of Defense, NASA, the commercial aircraft industry, and numerous scientific advisory committees throughout the 1960s and early 1970s. These needs were subsequently summarized in a 1971 report by the Advisory Group for Aerospace Research and Development (AGARD) which stated the group “held a Specialists’ Meeting in Paris on ‘Transonic Aerodynamics’ in recognition of the fact that the absence of adequate theoretical methods and wind tunnels of high enough Reynolds number had already led to costly shortcomings in the transonic performance of certain combat and transport aircraft” [8]. Thus began an approximately 15 year process to design, source, fabricate, and commission the facility. Multiple workshops with future partners and customers were held to ensure the NTF met the need for high Reynolds number testing [2, 3, 7]. The outcome of these workshops and studies identified opportunities for technology improvements. The development of such a facility required advances in materials, tunnel manufacturing techniques, instrumentation, test techniques, and model fabrication.

Upon identification of key testing requirements and desired capabilities, conceptual design started in 1972. These efforts yielded configurations that were down-selected to a high-pressure Ludwieg tube or a cryogenic nitrogen facility [6]. As has been documented, five key requirements resulted in the cryogenic tunnel concept including [2, 7]

- 1) strong dependence of Reynolds number as a function of temperature at low temperatures
- 2) increase the maximum Reynolds number that can be tested
- 3) reduced temperature yields decreased speed of sound, requiring lower velocity air speed and thus reduced power draw
- 4) cryogenic nitrogen gas is similar to ambient, high-altitude flight conditions when compared to non-cryogenic high-pressure nitrogen or air
- 5) independent control of total pressure, total temperature, and fan speed yields independent behavior of flow regime (Reynolds number), compressibility (Mach), and dynamic pressure (aeroelastic effects)

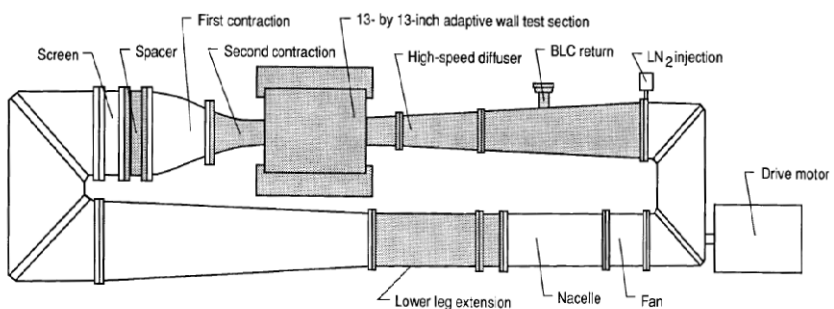
In particular, the cryogenic facility was selected due to the continuous operation and independent control of Mach, Reynolds number, and dynamic pressure. The aerodynamic flowfield fundamentally responds to both Mach and Reynolds number. Aeroelastics, which can be a significant factor, is a function of dynamic pressure. The ability to match Reynolds number and Mach number at a given dynamic pressure was unique and revolutionary. Following selection of the cryogenic nitrogen concept, detailed design commenced in 1974 [3] and finalized the facility requirements in 1975.

A great deal of research and development led to the construction of the NTF. In Fall 1971, a small group of engineers started to investigate cryogenic wind tunnel capabilities and constructed two risk-reduction facilities [9–11]. First, a low-speed, low-temperature facility was constructed to evaluate the effectiveness of liquid nitrogen injectors and also material behavior at low temperatures. This low-speed, low-temperature atmospheric, fan-driven wind tunnel had a rectangular 7 in by 11 in (17.8 cm by 27.9 cm) test section and operated from 300 K (140 deg F, 60 deg C) down to 80 K (-316 deg F, -193 deg C) at Mach numbers from near 0 to 0.2 [9]. This testbed confirmed that liquid nitrogen injectors could be used to successfully achieve stable cryogenic conditions. Confidence in this facility led to the design and construction of the small transonic, cryogenic, closed-circuit Langley 0.3-Meter Transonic Cryogenic Tunnel, one of numerous outcomes from the NTF Activation Technology Development Program. An image of the circuit and test section can be seen in Fig. 1 [4, 10]. This facility, opened in August 1973, served as a test bed to confirm transonic, cryogenic conditions and develop requisite instrumentation for the NTF. The wind tunnel, containing a 0.3-meter by 0.3-meter test section, originally designed to operate for 90 days, is still in active use for technology-development experiments, more than 50 years after the original construction.

Following these two proof-of-concept facilities, permission was granted in 1975 to develop a large-scale, continuous-flow, pressurized, cryogenic nitrogen wind tunnel at NASA Langley Research Center [7], for which congressional funding was appropriated in 1976. Facility construction began in 1979 and was completed in 1982, and an aerial view of the completed facility is pictured in Fig. 2. More than two years were then invested to ensure the facility was ready for production usage, which was granted in late 1984. Originally, details of the facility were not publicly discussed or disseminated, but increased international and public interest in the facility led to much information being released in the early 2000s.



(a) contraction, test section, and diffuser



(b) circuit

Fig. 1 Langley 0.3-meter Transonic Cryogenic Tunnel [source: NASA].

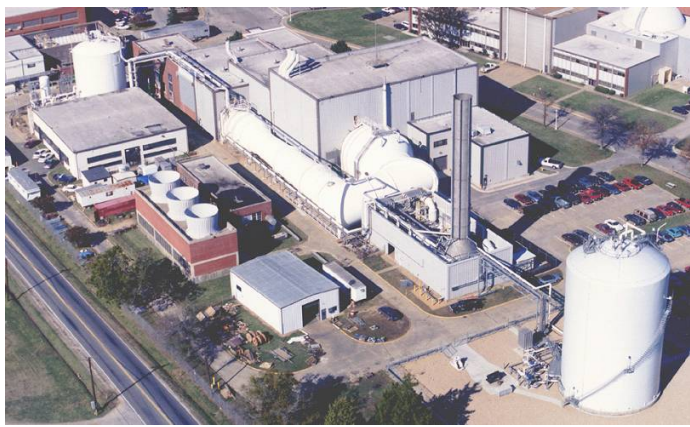


Fig. 2 Aerial view of the National Transonic Facility [source: NASA].

While the NTF is a United States physical asset, many international partners have collected valuable and unique data at the facility. Some of these nations also assisted in the design and fabrication of the wind tunnel through workshops, consultation, and supplying materials [2, 5, 7]. While many materials were manufactured in the United States, it is noteworthy that some of the steel was made by Japan Steel Works, Ltd. (“Japan Steel” or “JSW”). Prior to the selection of a vendor, Japan Steel developed 9% Nickel maraging steel, which was shown to have superior strength and fatigue life than conventional maraging steel. In addition to developing improved material chemical properties, Japan Steel developed methods to make steel up to 1.3 ft (0.40 m) thick [12]. It has been stated that “[c]onsidering that the current ASTM specifications for 9% Nickel limit thickness to 0.13 m, Japan Steel made a quantum jump in state-of-the-art manufacturing 9% Nickel steel in heavy sections” [12]. At the time of material sourcing, Japan Steel was able to manufacture strong steel with larger forges and thicker material than domestically available [12, 13]. The size of disk forging is limited by both the diameter of the press, driven by the distance between the support posts, and the tonnage of the press. It was found that Japan Steel was able to forge the strong steel with a maximum forge diameter of 12.0 ft (3.66 m), which is of the requisite scale for the materials and larger than anything available in the United States at the time. While not all facility steel was provided by Japan Steel, both the model support and fan drive shaft were made from this high-strength 9% Nickel. This hardware was transported across the Pacific Ocean on the deck of a shipping vessel, and high-strength steel was needed to avoid damage during shipment [14]. Consequently, the ultimate strength was selected to ensure hardware integrity in shipment in addition to meeting facility requirements. Despite being routinely stated, it is an urban legend that a domestic shortage of steel required Japan Steel to manufacture the steel. That is to say that Japan Steel was selected due to technological capabilities and not a material shortage. After completion of the facility, a samurai sword was manufactured by Japan Steel swordship shop and provided to NASA as a token of appreciation and symbol of international collaboration [15]. This sword, shown in Fig. 3 is on display in the NTF building. The sword was generated by Japan Steel master swordsmith Tanetsugu Horii in accordance with



Fig. 3 Samurai sword presented by Japan Steel on display in the NTF building [source: NASA].

Japanese tradition and manufacturing techniques. This sword is on display in the NTF building, and the accompanying informational sign indicates the sword was provided “in hope that this sword would serve as a symbol of the international cooperation reflected in the National Transonic Facility.”

Figure 4 shows the NTF wind tunnel circuit in which flow travels in a counter-clockwise direction. Beginning in the top right, a subsonic fan accelerates the flow. A low-speed diffuser section, including Turns 3 and 4, slowly decelerates the flow until just before the settling chamber. At this point, a wide-angle diffuser then leads into the four anti-turbulence screens. After the settling chamber, the flow is rapidly accelerated up to the test section, which contains 12 wall slots and corresponding reentry flaps on the floor and ceiling to enable transonic and supersonic flow. Upon exiting the test section, the high-speed diffuser leads into Turn 1 after which liquid nitrogen is injected into the flow for cryogenic operation. Upon moving through Turn 2, the flow is again accelerated through the fan, and the circuit is complete. A green, shaded region of the circuit depicts the portion of the wind tunnel geometry that has been released. This section includes the end of the settling chamber, contraction region, test section, and high-speed diffuser. The plenum, shown in blue, surrounds the test section and has also been released. In addition to the facility, the upper-swept strut and arc sector mounting hardware have both been released.

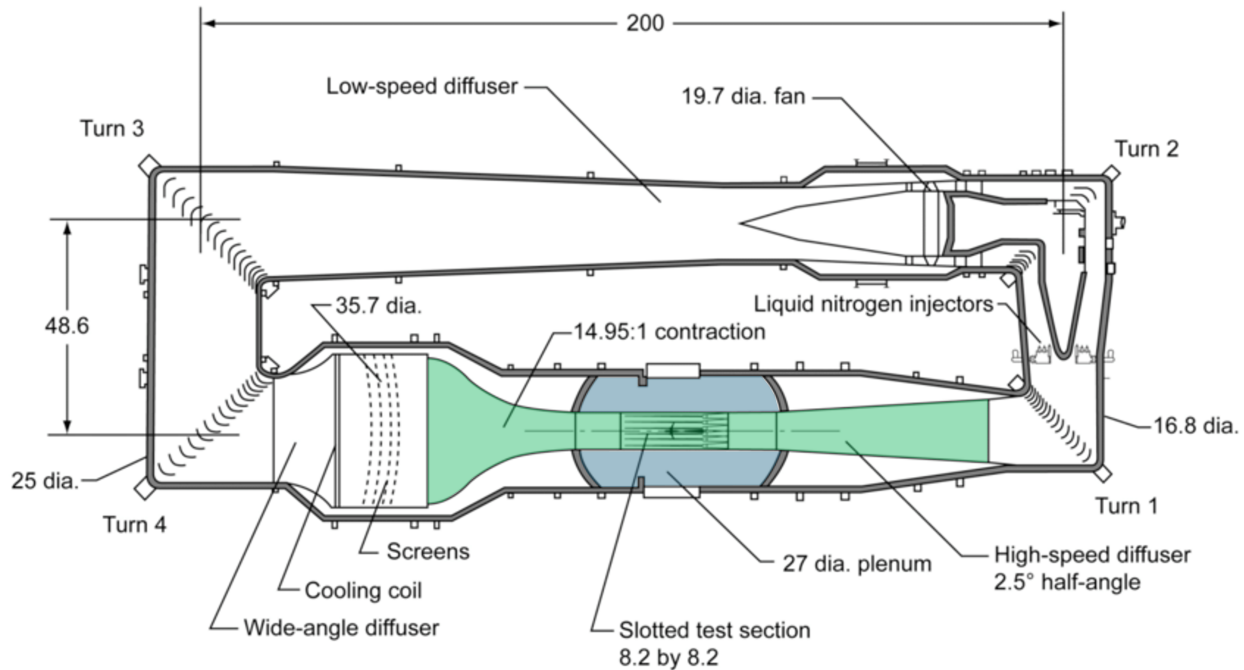


Fig. 4 NTF test circuit and released geometry (green and blue), units in feet.

III. Facility Digitization

A digital model of the NTF was generated with a high-density laser scan and careful manipulation of the resulting point cloud into clean computer-aided design (CAD) surfaces [16, 17]. Key components of the high-speed leg of the facility include the outer shell, contraction, test section, slots and flaps, high-speed diffuser, model support hardware, and the plenum surrounding the test section. The slot size in the tunnel walls can be set to either 6% open (the standard facility geometry), 4% open, or 0% open (fully closed). The point cloud was collected with the standard 6% open. NTF Test 229, one of three NTF CRM tests, investigated the effect of these slot opening sizes. Most runs were completed with slot openings of 6%, which is consistent with other NTF CRM tests. Multiple other runs were executed with slot covers installed on the walls (i.e., 0% open). Some other tests were executed with the middle slots fully closed and the other four slots fully open. A final set of runs was executed with fully-closed middle and outboard-most slots, leaving just the second and fifth slots fully open. Again, it is emphasized that the point cloud was collected with the 6% open slots.

CAD was generated from the “as-built” geometry as opposed to “as-designed” to allow the most accurate comparisons between the facility experimental data and computational simulations. The Geographic Information System group captured a 251 million point cloud, of which about 80% was captured in the plenum, due to the large number of features in the plenum. These point cloud data were subsequently manipulated by the GEOLAB group, including two of the co-authors for this paper. Data manipulation was performed with the GeoMagic software package. Ultimately, these data were combined with physical inspection of the facility, photographs, construction drawings, and engineering judgment to create the resulting CAD surfaces.

IV. Common Research Model Tests

While a plethora of models have been tested in the NTF, particular attention in this paper is drawn to the NASA Common Research Model and two of its derivatives. The first three Drag Prediction Workshops (DPW-I through DPW-III) compared state-of-the-art computational methods to experimental data that were collected decades previously, and the need for industry-relevant, high-quality data was a key outcome of DPW-III. Consequently, the American Institute of Aeronautics and Astronautics (AIAA) Applied Aerodynamics Technical Committee requested the development of a publicly-available, industry-relevant, general commercial transport vehicle, which resulted in the NASA Common Research Model (CRM) [18–21]. This vehicle has been used for DPW-IV through the upcoming DPW-8. It has also been extensively studied by academic, government, and industry partners, and this is the most widely-studied commercial transport vehicle. The CRM, designed for Mach 0.85, has been tested three times in NTF test campaigns NTF-197, NTF-215, and NTF-229 [21–24]. These experimental data have revolutionized the aerodynamics field by enabling high-quality comparisons between experimental and computational data. While the original intent of the CRM was to enable detailed comparisons for the DPW series, the influence and legacy of the CRM extends far beyond DPW.

With the success of the CRM and DPW series, attention was turned to other flight regimes, and the AIAA High-Lift Prediction Workshop (HLPW) was conceived. Similar to the CRM, an industry-relevant low-speed, high-lift vehicle was needed to enable high-quality comparisons between experimental and HLPW computations [25]. The High Lift CRM (CRM-HL) is a derivative of the CRM that contains slats and flaps to enable comparisons in both takeoff and landing configurations. The original CRM was designed for transonic flight with no high-lift design considerations. Consequently, some design modifications to the sectional airfoils geometry, twist, and shear were made for high-lift considerations. Due to high-lift flowfield complexities, detailed comparisons have required extensive test campaigns in multiple facilities [26]. A significant amount of the computational data has been compared to the Office National d’Études et de Recherches Aérospatiales (ONERA) F1 low-speed wind tunnel and the NASA LaRC 14- by 22-Foot Subsonic Tunnel (14x22). A recent 2023-2024 NTF test campaign (NTF-237) will supplement these data. One reference for this test has been published to date, and a special session at AIAA Aviation 2025 will contain more papers about the model and test [27].

A third variant of the CRM, the Natural Laminar Flow Common Research Model (CRM-NLF) has also been tested in the NTF [28, 29]. The CRM-NLF was designed for a transonic design point at Mach 0.85 with the original CRM planform, but the airfoil sections were designed to enable transonic, swept-wing, natural laminar flow [29, 30]. Facility and testing improvements for NTF-228 were necessary to capture the laminar flow characteristics. In particular, a new carbon-based heating temperature-sensitive paint was applied to the model to capture the laminar flow extent [28]. These novel experimental results have enabled detailed comparisons between computational and experimental data for an industry-relevant, transonic, swept-wing, natural laminar flow geometry. It is anticipated that these data will continue to be used for transition-prediction comparisons and methods development.

V. CRM Coordinate System Transformations

Building off of Sec. IV, coordinate system transformations for the full-scale CRM into wind-tunnel coordinates is particularly important. Coordinate transformations in this section present the transformations as currently understood and reflected in version 1.9 of the NTF geometry. It is possible that constants in the subsequent equations will change with additional interrogation, and thus the transformations below should not be taken as truth. Consult the `how_mounted*` files for the up-to-date transformations. Transformations in this section are only applicable to the CRM family of vehicles. While other models rotate about $(x, z) = (156, 0)$, the arithmetic to go from full-scale to model-scale will not be the same.

The coordinate systems below include full-scale (fs) vehicle, model-scale (ms) vehicle, wind-tunnel (wt), zero angle-of-attack (za) vehicle, and the analysis coordinates (ac). All values in this section are in inches. The arc sector is able to rotate a maximum of 11 deg up (negative α) and 19 deg down (positive α) in which α is the angle of attack. The sidewall-mounted hardware allows the vehicle to pitch 28 deg up (positive α) and 28 deg down (negative α). A visualization of the full-span vehicle, strut, and arc sector is shown in Fig. 5(a) showing the CRM mounted on the upper-swept strut. Some simplifications were made to the outer shell (shown in gold). As seen in Fig. 5(b,c), the arc sector can pierce this simplified outer shell at large angles of attack. Although this is not real (in reality there are protrusions where the rotated arc sector can fit), this is occurring in an area well away from the region of interest, and thus can be neglected. The arc sector does not move for the sidewall-mounted models, so the pierced sidewall is not a consideration.

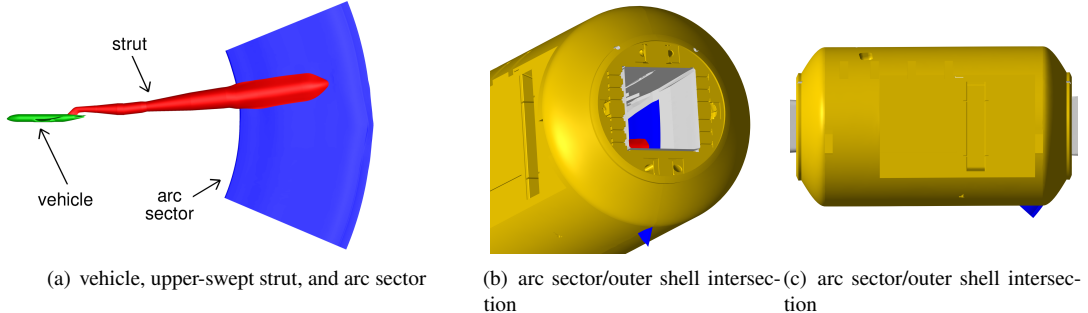


Fig. 5 Facility mounting hardware and key components.

A. Full-Span Strut-Mounted 2.7%-Scale CRM and CRM-HL

The transformation of the 2.7%-scale vehicle, whether the traditional high-speed CRM or CRM-HL, mounted on the upper-swept strut is as follows:

- Eqn. 1: scale the full-scale vehicle to model-scale
- Eqn. 2: translate the model-scale vehicle to the wind-tunnel coordinate system origin at $(120.201, 0, -4.805)$
- Eqn. 3: rotate the arc sector and upper-swept strut, but not the vehicle, -6.43 deg about the tunnel centerline y axis for the rotation origin (O) at $(156, 0, 0)$
- Eqn. 4: for non-zero angle of attack cases, rotate the arc sector, upper-swept strut, and vehicle about the tunnel centerline y axis for the rotation origin (O) at $(156, 0, 0)$

In a mathematical formulation, the transformations can be defined transforming the full-scale vehicle to model scale by

$$\begin{bmatrix} x \\ y \\ z \end{bmatrix}_{ms} = 0.027 \begin{bmatrix} x \\ y \\ z \end{bmatrix}_{fs} \quad (1)$$

and then from the model scale origin to the wind-tunnel origin via

$$\begin{bmatrix} x \\ y \\ z \end{bmatrix}_{wt} = \begin{bmatrix} x \\ y \\ z \end{bmatrix}_{ms} + \begin{bmatrix} 120.201 \\ 0 \\ -4.805 \end{bmatrix} \quad (2)$$

which is followed by rotating the arc sector and upper-swept strut (“hardware”), but not the vehicle, to attach to the vehicle at $\alpha=0$ deg

$$\begin{bmatrix} x \\ y \\ z \end{bmatrix}_{za, \text{ hardware}} = \mathcal{R} \left\{ \theta = -6.43, \mathbf{v} = \begin{bmatrix} 0 \\ 1 \\ 0 \end{bmatrix}_{O=(156,0,0)} \right\} \cdot \begin{bmatrix} x \\ y \\ z \end{bmatrix}_{wt} \quad (3a)$$

$$\begin{bmatrix} x \\ y \\ z \end{bmatrix}_{za, \text{ vehicle}} = \begin{bmatrix} x \\ y \\ z \end{bmatrix}_{wt} \quad (3b)$$

in which \mathcal{R} represents the rotation matrix of an angle θ rotated around a vector \mathbf{v} . Ultimately, moving to the analysis coordinates at a non-zero α is done with

$$\begin{bmatrix} x \\ y \\ z \end{bmatrix}_{ac} = \mathcal{R} \left\{ \alpha, \mathbf{v} = \begin{bmatrix} 0 \\ 1 \\ 0 \end{bmatrix}_{O=(156,0,0)} \right\} \cdot \begin{bmatrix} x \\ y \\ z \end{bmatrix}_{za} \quad (4)$$

It may be useful to check one’s work with the provided equations. The nose of the full-scale CRM is located at (92.5, 0, 198), and the above-listed equations move the nose to (122.6985, 0.0000, 0.5410) for α of 0 deg.

B. Semispan Sidewall-Mounted 5.2%-Scale CRM-HL and CRM-NLF

A sidewall-mounted 5.2%-scale model has also been tested. When looking downstream, the semispan model is located on the left side of the tunnel and thus uses the port wing geometry. The sidewall-mounted 5.2%-scale vehicle transformations are as follows. To maintain consistency with the 2.7%-scale sidewall-mounted model, discussed in the next subsection, the vehicle is translated and scaled to the wind-tunnel coordinate system in one step. This is contrary to the 2.7% full-span vehicle which is scaled and then translated. The above-listed 2.7% full-span coordinates have been published for multiple years, and thus the equations for that transformation will not be updated. However, both the 5.2% and 2.7% sidewall models are translated and scaled in one step for maximum clarity and consistency. Note that the -6.43 deg rotation to align with the upper swept strut is not needed for the sidewall-mounted vehicle. In this configuration, a straight stubsting and camera pod bullethead fairing are attached to the arc sector. These coordinate transformations require an approximately 2.00 in offset between the vehicle centerline and the sidewall. This value is a result of a standoff plate and labyrinth seal, which is used to minimize flow between the model and the standoff plate, between the vehicle and sidewall. For more details, consult Ref. [31]. The offset plate is not included for integrated force and moments. The coordinate transformations are as follows:

- Eqn. 5: translate and scale the full-scale vehicle to the wind-tunnel coordinate system
- Eqn. 6: no additional hardware rotation is needed to achieve $\alpha=0$ deg, unlike the upper-swept strut mounted vehicle
- Eqn. 7: for non-zero angle of attack cases, rotate the vehicle about the tunnel centerline y axis for the rotation origin (O) at (156,0,0)

The equations for the transformations begin by translating and scaling the vehicle to the wind tunnel center of rotation and scale with

$$\begin{bmatrix} x \\ z \end{bmatrix}_{wt} = \left(\begin{bmatrix} x \\ z \end{bmatrix}_{fs} + \begin{bmatrix} -1244.09615 \\ -217.09615 \end{bmatrix} \right) 0.052 + \begin{bmatrix} 156 \\ 0 \end{bmatrix} \quad (5a)$$

$$y_{wt} = (-y_{fs}) 0.052 + (49.24257 - t_s) \quad (5b)$$

in which t_s is the standoff distance. This value is 2.0 in for the 5.2% scale model, which includes both the offset plate and labyrinth seal. Contrary to the arc sector configuration, no additional hardware rotation is required to reach 0 angle of attack, and thus

$$\begin{bmatrix} x \\ y \\ z \end{bmatrix}_{za} = \begin{bmatrix} x \\ y \\ z \end{bmatrix}_{wt} \quad (6)$$

Analysis at non-zero α is done with

$$\begin{bmatrix} x \\ y \\ z \end{bmatrix}_{ac} = \mathcal{R} \left\{ \alpha, \mathbf{v} = \begin{bmatrix} 0 \\ 1 \\ 0 \end{bmatrix}_{O=(156,0,0)} \right\} \cdot \begin{bmatrix} x \\ y \\ z \end{bmatrix}_{za} \quad (7)$$

Similar to the previous model, a check may be warranted between one's work and the provided equations. The nose of the full-scale CRM is located at (92.5, 0, 198), and the above-listed equations rig the 5.2% semispan model nose at (96.1170, 47.2426, -0.9930) for α of 0 deg.

C. Semispan Sidewall-Mounted 2.7%-Scale CRM-HL

While not yet tested, there are plans to test a 2.7%-scale sidewall-mounted CRM-HL. This model is connected to the same mounting hardware as the 5.2%-scale model previously discussed, and thus the transformations are very similar to those presented in Sec. V.B. However, the translations along the x and z axes are different than the larger model. In addition, the 2.7%-scale model includes a 1.0 inch standoff and labyrinth seal assembly. Conceptually, the transformations are applied by:

- Eqn. 8: translate and scale the full-scale vehicle to the wind-tunnel coordinate system
- Eqn. 9: no additional hardware rotation is needed to achieve $\alpha=0$ deg, unlike the upper-swept strut mounted vehicle
- Eqn. 10: for non-zero angle of attack cases, rotate the vehicle about the tunnel centerline y axis for the rotation origin (O) at (156,0,0)

The equations for the transformations begin by translating and scaling the vehicle to the wind tunnel center of rotation and scale with

$$\begin{bmatrix} x \\ z \end{bmatrix}_{wt} = \left(\begin{bmatrix} x \\ z \end{bmatrix}_{fs} + \begin{bmatrix} -1354.81482 \\ -217.03704 \end{bmatrix} \right) 0.027 + \begin{bmatrix} 156 \\ 0 \end{bmatrix} \quad (8a)$$

$$y_{wt} = (-y_{fs}) 0.027 + (49.24257 - t_s) \quad (8b)$$

in which t_s is 1.0 in for the 2.7% sidewall model. This value includes the standoff and labyrinth seal. Contrary to the arc sector configuration, no additional hardware rotation is required to reach 0 angle of attack, and thus

$$\begin{bmatrix} x \\ y \\ z \end{bmatrix}_{za} = \begin{bmatrix} x \\ y \\ z \end{bmatrix}_{wt} \quad (9)$$

Analysis at non-zero α is done with

$$\begin{bmatrix} x \\ y \\ z \end{bmatrix}_{ac} = \mathcal{R} \left\{ \alpha, \mathbf{v} = \begin{bmatrix} 0 \\ 1 \\ 0 \end{bmatrix}_{O=(156,0,0)} \right\} \cdot \begin{bmatrix} x \\ y \\ z \end{bmatrix}_{za} \quad (10)$$

The full-scale CRM nose, located at (92.5, 0, 198), is thus moved to (121.9175, 48.2426, -0.5140) for α of 0 deg.

VI. Released Geometry Files

The NTF geometry is hosted on the Drag Prediction Workshop (DPW) website, currently at <https://aiaa-dpw.larc.nasa.gov/ntf.html>. The following steps should be taken to load in the NTF test section geometry

- 1) load empty NTF test section parts

- NTF_Contraction_TestSection_Diffusor_2023_10_02.igs
- optional: NTF_Additional_Obstructions_2023_10_02.igs (with camera pod)

- 2) add the arc sector (for both full-span and semispan models)
 - NTF_arc_sector_aft_fixed.igs
 - NTF_arc_sector_fwd_rotational_0deg.igs; roate arc sector -6.43 deg around the y-axis at rotation point (156 , 0, 0)
- 3) option 1: add full-span model and upper-swept strut
 - NTF_USS_Sting_noRotation_2025_04_21.igs; rotate upper-swept strut -6.43 deg around the y-axis at (156 , 0, 0)
 - if using the CRM geometry; mirror the vehicle around the fuselage centerline and apply coordinate transformations in Sec. V.
- 4) option 2: add semispan wall model and camera pod
 - NTF_Arc_Sector_CameraPod_2023_10_02.igs
 - if using the CRM geometry; mirror the vehicle around the fuselage centerline and apply coordinate transformations in Sec. V

The computer aided design (CAD), available in a single zip file, includes twelve parts in three formats (*.stp, *.iges, and *.x_t). Images of these 12 parts and visualization of the geometry are shown in Figs. 6–9. In alphabetical order, the 12 files are as follows:

- Individual_Parts/NTF_Diffusor_2023_10_02.igs
- Individual_Parts/NTF_Inlet_Contraction_2023_10_02.igs
- Individual_Parts/NTF_TestSection_Baseline_in_Plenum_2023_10_02.igs
- NTF_Additional_Obstacles_2025_05_27.igs
- NTF_Arc_Sector_Aft_Fixed.igs
- NTF_Arc_Sector_CameraPod_2023_10_02.igs
- NTF_Arc_Sector_Fwd_Rotational_0deg.igs
- NTF_Arc_Sector_Rotational_Axis_Cylinder_2023_10_02.igs
- NTF_Arc_Sector_Straight_Sting_0deg_2023_10_02.igs
- NTF_Contraction_TestSection_Diffusor_2023_10_02.igs
- NTF_Diffusor_Constant_Cross_Section_Extension_2023_10_02.igs
- NTF_USS_Sting_noRotation_2025_04_21.igs

VII. Conclusions

Digital geometry for the NASA National Transonic Facility has been released and is available for public use. A detailed scan was performed of the full wind tunnel circuit, and key components of the facility have been cleared for public use. This includes the contraction after the settling chamber, the test section and surrounding plenum, outer shell, and the high-speed diffuser. High-quality computer-aided design files are available, which include detailed features such as the slots and gaps in the walls. Mounting hardware, including the upper-swept strut and arc sector, is also available for download. This geometry will be an integral part of Drag Prediction Workshop 8, scheduled for 2026. The geometry can be freely downloaded from the Drag Prediction Workshop website.

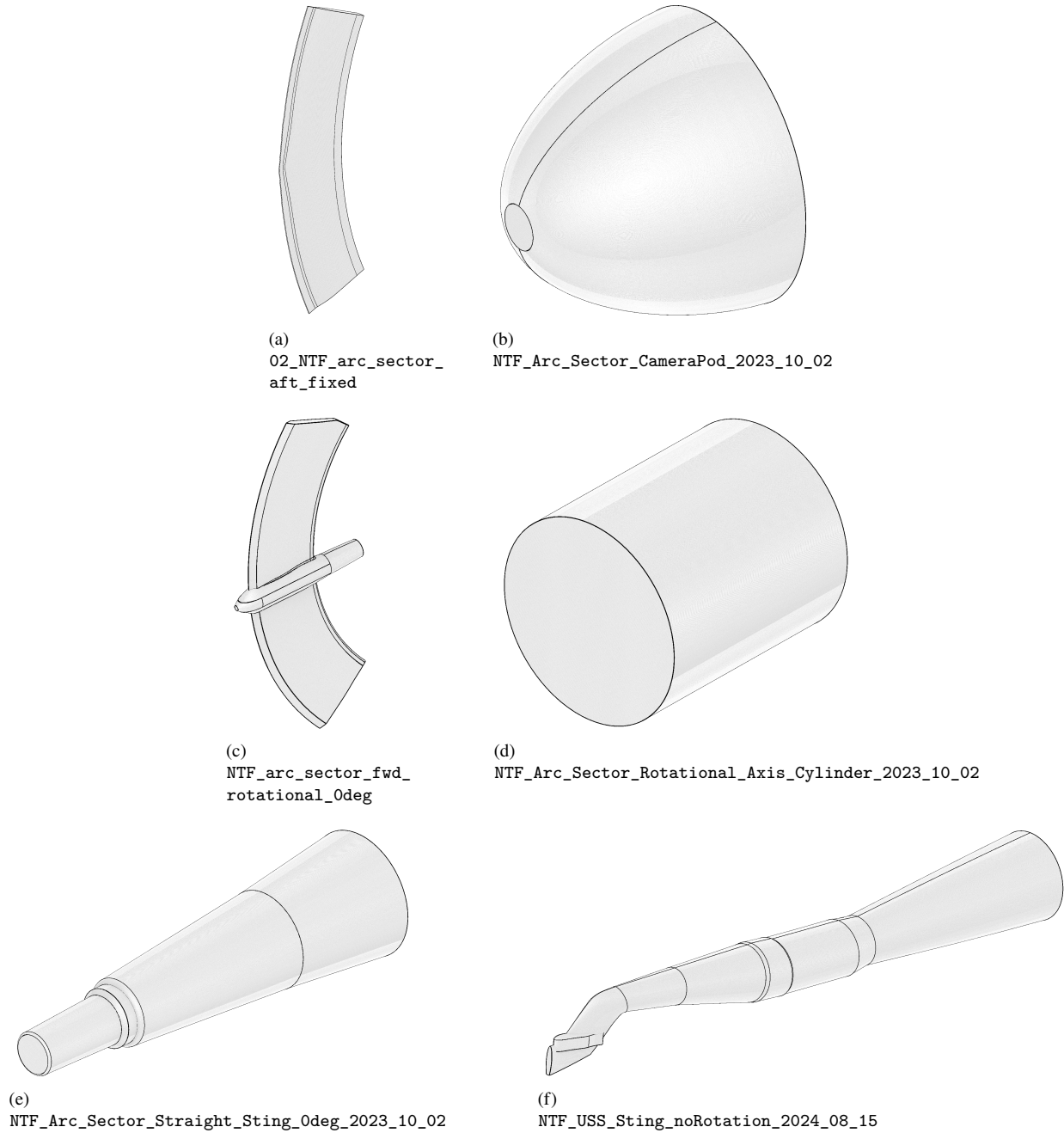


Fig. 6 NTF model mounting hardware.

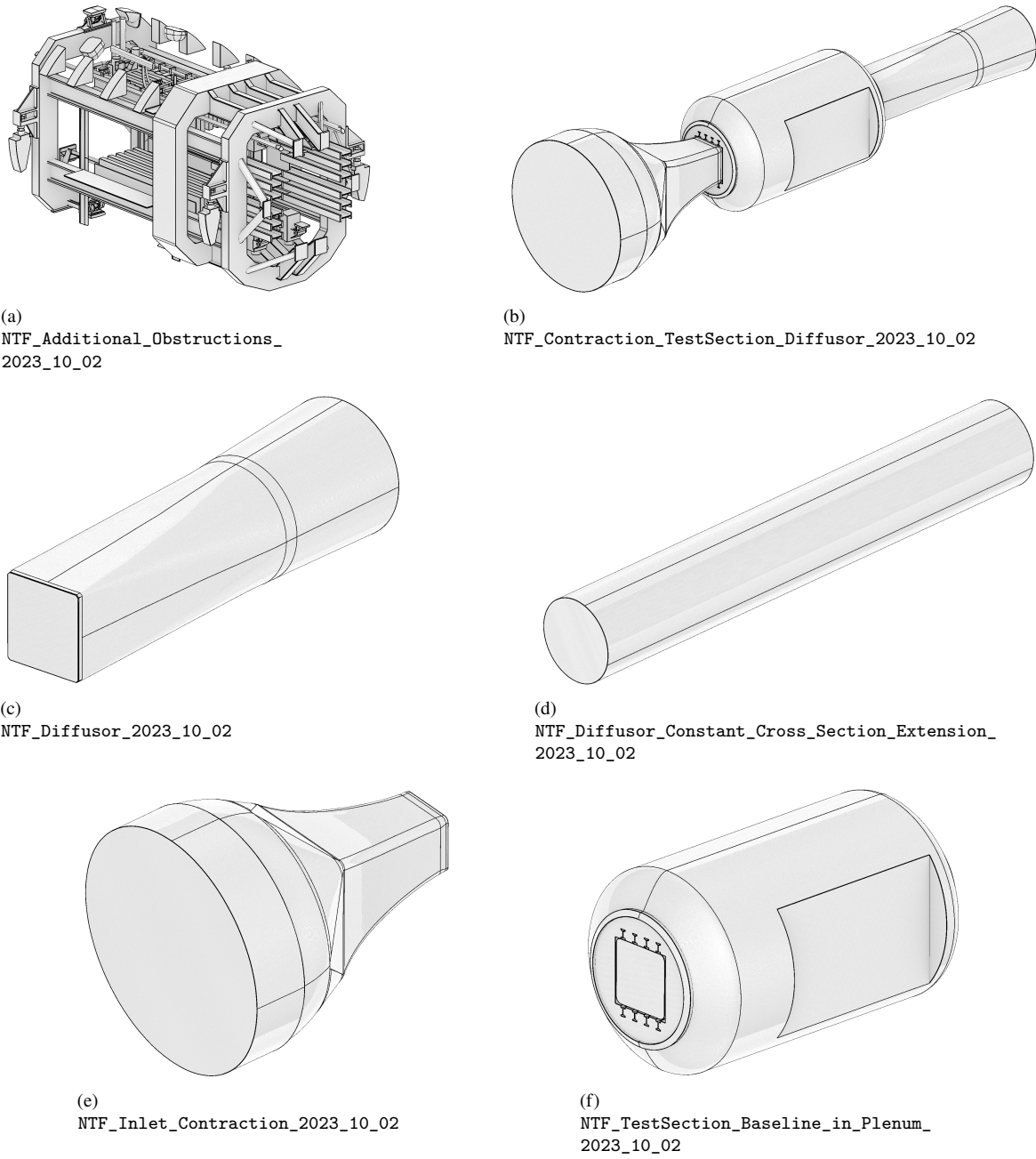


Fig. 7 Wind tunnel and test section geometry.

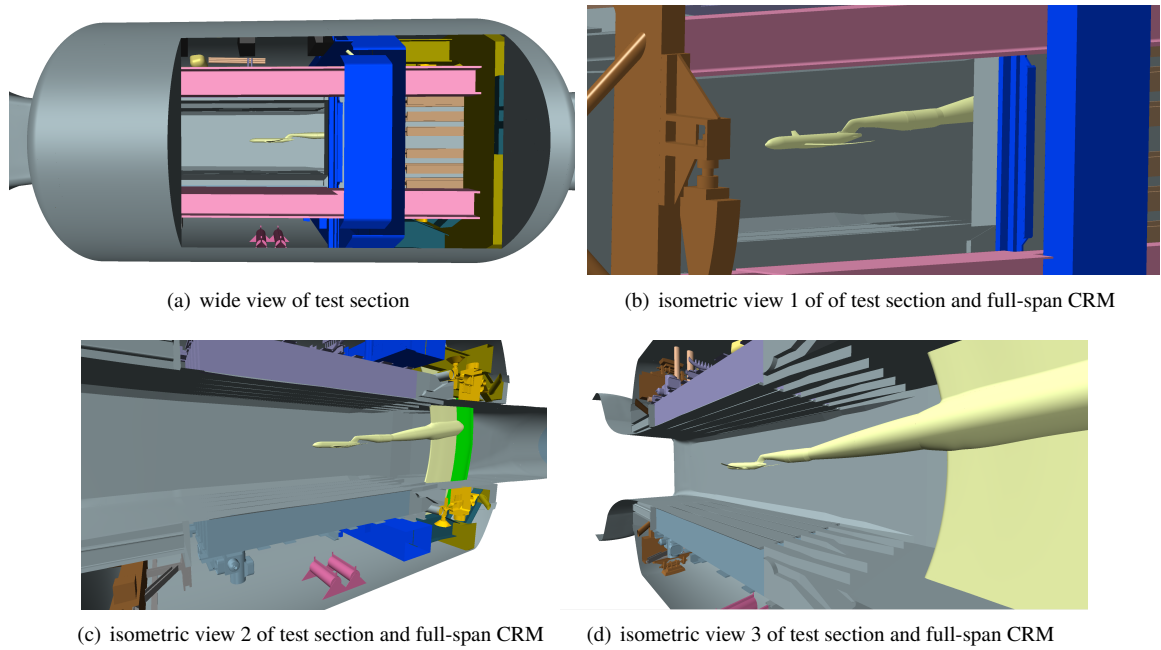


Fig. 8 NTF assembly.

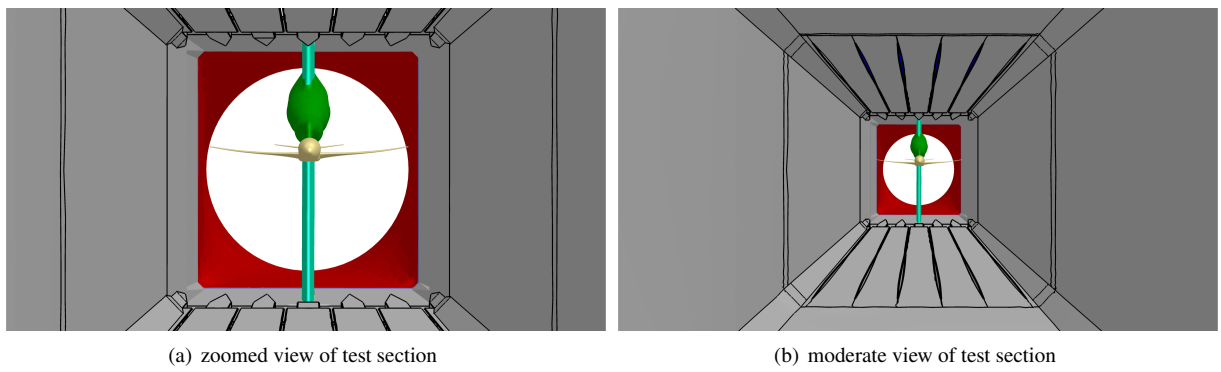


Fig. 9 Interior of NTF assembly.

References

- [1] Bisset, Jr., O. W., “NASA’s Aeronautic Test Program: National Transonic Facility,” March, 2015. https://www.nasa.gov/wp-content/uploads/2015/12/m187007_ntfprint_508.pdf.
- [2] Wahls, R. A., “The National Transonic Facility: A Research Retrospective (Invited),” AIAA Paper 2001-0754, Aerospace Sciences Meeting and Exhibit, Reno, NV, 2001.
- [3] Howell, R. R., “Overview of Engineering Design and Operating Capabilities of the National Transonic Facility,” *NASA Conference Publication 2122, Part I: Cryogenic Technology: Proceedings of a conference held at Langley Research Center, Hampton, Virginia*, November 27-29, 1979, pp. 49–76.
- [4] McKinney, L. W., and Gloss, B. B., “Status of the National Transonic Facility,” AIAA Paper 82-0604, Aerodynamic Testing Conference, Williamsburg, VA, 1982.
- [5] Campbell, J. F., “The National Transonic Facility: A Research Perspective,” AIAA Paper 84-2150, Applied Aerodynamics Conference, Seattle, WA.
- [6] Wahls, R. A., “Role of Cryogenic Aerodynamic Testing for Current and Future Technologies,” US Patent and Trademark Office Patent Examiner Technical Training Program, 2021.
- [7] Young, Jr., C. P., and Gloss, B. B., “Cryogenic Wind Tunnel Models,” NASA Conference Publication 2262, Cryogenic Wind Tunnel Models Workshop, 1982.
- [8] “Facilities and Techniques for Aerodynamic Testing at Transonic Speeds and High Reynolds Numbers,” AGARD CP-83-71, 1971.
- [9] Kilgore, R. A., “Design Features and Operational Characteristics of the Langley 0.3-Meter Transonic Cryogenic Tunnel,” *NASA Technical Note D-8304*, December, 1976.
- [10] Kilgore, R. A., “Evolution of the Cryogenic Wind Tunnel and Experience with the Langley 0.3-Meter Transonic Cryogenic Tunnel,” *NASA Conference Publication 2122, Part I: Cryogenic Technology: Proceedings of a conference held at Langley Research Center, Hampton, Virginia*, November 27-29, 1979, pp. 3–48.
- [11] Lawing, P. L., Dress, D. A., and Kilgore, R. A., “Description of the Insulation System for the Langley 0.3-Meter Transonic Cryogenic Tunnel,” NASA Technical Memorandum 86274, January, 1985.
- [12] Wingate, R. T., “Design of Compressor Fans for Large Cryogenic Wind Tunnels,” *NASA Conference Publication 2122, Part I: Cryogenic Technology: Proceedings of a conference held at Langley Research Center, Hampton, Virginia*, November 27-29, 1979, pp. 157–167.
- [13] Young, Jr., C. P., Gerringer, A. H., Brooks, T. G., and Berry, Jr., R. F., “Nine Percent Nickel Steel Heavy Forging Weld Repair Study,” *NASA Technical Memorandum 78738*, July, 1978.
- [14] Gloss, B. B., *Correspondance with the author: NTF Japan Steel history question*, March 19, 2025.
- [15] Tateno, M., and Japan Steel Works, Informational display in the NTF facility. March, 1984.
- [16] Rivers, S. M., Nayani, S. N., Tinetti, A. F., Brynildsen, S. E., and Ferris, R. J., “Numerical Study of the High-Speed Leg of the National Transonic Facility,” STO-MP-AVT-284-13, March, 2018.
- [17] Elmiligui, A., Rivers, S. M., and Walker, E., “Numerical Simulation of the High-Speed Leg of the National Transonic Facility,” STO-MP-AVT-338, March, 2021.
- [18] Vassberg, J. C., DeHaan, M. A., Rivers, S. M., and Wahls, R. A., “Development of a Common Research Model for Applied CFD Validation Studies,” AIAA Paper 2008-6919, AIAA Applied Aerodynamics Conference, Honolulu, HI 2008.
- [19] Vassberg, J. C., Tinoco, E. N., Mani, M., Rider, B., Zickuhr, T., Levy, D. W., Brodersen, O. P., Eisfeld, B., Crippa, S., Wahls, R. A., Morrison, J. H., Mavriplis, D. J., and Murayama, M., “Summary of the Fourth AIAA CFD Drag Prediction Workshop,” AIAA Paper 2010-4547, AIAA Applied Aerodynamics Conference, Chicago, IL, 2010.
- [20] Vassberg, J. C., DeHaan, M. A., Rivers, M. B., and Wahls, R. A., “Retrospective on the Common Research Model for Computational Fluid Dynamics Validation Studies,” *Journal of Aircraft*, Vol. 55, No. 4, 2019, pp. 1325–1337.
- [21] Rivers, M. B., “NASA Common Research Model: A History and Future Plans,” AIAA Paper 2019-3725, AIAA Aviation Forum, Dallas, TX, 2019.

- [22] Rivers, M. B., and Dittberner, A., "Experimental Investigation of the NASA Common Research Model," AIAA Paper 2010-4218, AIAA Applied Aerodynamics Conference, Chicago, IL, 2010.
- [23] Rivers, M. B., and Dittberner, A., "Experimental Investigations of the NASA Common Research Model in the NASA Langley National Transonic Facility and NASA Ames 11-Ft Transonic Wind Tunnel," AIAA Paper 2011-1126, AIAA Aerospace Sciences Meeting, Orlando, FL, 2011.
- [24] Rivers, M. B., Quest, J., and Rudnik, R., "Comparison of the NASA Common Research Model European Transonic Wind Tunnel Test Data to NASA Test Data," AIAA Paper 2015-1093, AIAA SciTech Forum, Kissimmee FL, 2015.
- [25] Lacy, D. S., and Sclafani, A. J., "Development of the High Lift Common Research Model (HL-CRM): A Representative High Lift Configuration for Transonic Transport," AIAA Paper 2016-0308, AIAA SciTech Forum, San Diego, CA, 2016.
- [26] Smith, A. M. O., "High-Lift Aerodynamics," *Journal of Aircraft*, Vol. 12, No. 6, 1975, pp. 501–530.
- [27] Langston, S. L., Winski, C. S., and Rivers, M. B., "Reynolds Number Effects on a 5.2%-Scale High Lift Common Research Model," AIAA Paper 2025-1514, AIAA SciTech Forum, Orlando, FL, 2025.
- [28] Rivers, M. B., Lynde, M., Campbell, R., Viken, S., Chan, D., Watkins, A. N., and Goodliff, S., "Experimental Investigation of the NASA Common Research Model with a Natural Laminar Flow Wing in the NASA Langley National Transonic Facility," AIAA Paper 2019-2189, AIAA SciTech Forum, San Diego, CA, 2019.
- [29] Banchy, M. N., and Campbell, R. L., "Computational Design and Analysis of a Transonic Natural Laminar Flow Wing for a Wind Tunnel Model," AIAA Paper 2017-3058, AIAA Aviation Forum, Denver, CO, 2017.
- [30] Campbell, R. L., and Lynde, M. N., "Building a Practical Natural Laminar Flow Design Capability," AIAA Paper 2017-3059, AIAA AVIATION Forum, Denver, CO, 2017.
- [31] Winski, C. S., Langston, S. L., Rivers, M. B., and Ertsgaard, M., "NASA 5.2%-Scale Semispan High Lift Common Research Model (CRM-HL) High Reynolds Number Wind Tunnel Test in the National Transonic Facility (NTF)," To be presented at AIAA AVIATION Forum, Las Vegas, NV, 2025.